Computational study of collisions between O(3P) and NO(2Π) at temperatures relevant to the hypersonic flight regime

Juan Carlos Castro-Palacio, Tibor Nagy, Raymond J. Bemish, and Markus Meuwly

Citation: The Journal of Chemical Physics **141**, 164319 (2014); doi: 10.1063/1.4897263

View online: http://dx.doi.org/10.1063/1.4897263

View Table of Contents: http://scitation.aip.org/content/aip/journal/jcp/141/16?ver=pdfcov

Published by the AIP Publishing

Computational study of collisions between O(^{3}P) and NO($^2\Pi$) at temperatures relevant to the hypersonic flight regime

Juan Carlos Castro-Palacio,[1] Tibor Nagy,[1,a)] Raymond J. Bemish,[2] and Markus Meuwly[1,b)]
[1]*Department of Chemistry, University of Basel, Klingelbergstrasse 80, CH-4056 Basel, Switzerland*
[2]*Air Force Research Laboratory, Space Vehicles Directorate, Kirtland AFB, New Mexico 87117, USA*

(Received 12 June 2014; accepted 24 September 2014; published online 29 October 2014)

Reactions involving N and O atoms dominate the energetics of the reactive air flow around spacecraft when reentering the atmosphere in the hypersonic flight regime. For this reason, the thermal rate coefficients for reactive processes involving O(^{3}P) and NO($^2\Pi$) are relevant over a wide range of temperatures. For this purpose, a potential energy surface (PES) for the ground state of the NO_2 molecule is constructed based on high-level *ab initio* calculations. These *ab initio* energies are represented using the reproducible kernel Hilbert space method and Legendre polynomials. The global PES of NO_2 in the ground state is constructed by smoothly connecting the surfaces of the grids of various channels around the equilibrium NO_2 geometry by a distance-dependent weighting function. The rate coefficients were calculated using Monte Carlo integration. The results indicate that at high temperatures only the lowest A-symmetry PES is relevant. At the highest temperatures investigated (20 000 K), the rate coefficient for the "O1O2+N" channel becomes comparable (to within a factor of around three) to the rate coefficient of the oxygen exchange reaction. A state resolved analysis shows that the smaller the vibrational quantum number of NO in the reactants, the higher the relative translational energy required to open it and conversely with higher vibrational quantum number, less translational energy is required. This is in accordance with Polanyi's rules. However, the oxygen exchange channel (NO2+O1) is accessible at any collision energy. Finally, this work introduces an efficient computational protocol for the investigation of three-atom collisions in general. © *2014 AIP Publishing LLC*. [http://dx.doi.org/10.1063/1.4897263]

I. INTRODUCTION

Nitric dioxide (NO_2) plays a major role in atmospheric chemistry, as a smog constituent and in combustion processes.[1–3] In the atmosphere, nitrous acid (HONO) can be generated from NO_2 through reaction with water which is important because HONO is a major source of OH leading to the formation of ozone and other air pollutants.[4,5] Depending on the chemistry involved, HONO formation from NO_2 can also involve reactants such as NO, water on surfaces[5] or soot surfaces.[6] While most of these processes occur close to thermal equilibrium and at moderate temperatures, reactions involving NO_2 have also attracted interest under more extreme conditions. This is the case for the hypersonic flight regime of spacecraft reentering the atmosphere. The chemistry near the surface of such vehicles typically involves highly non-equilibrium conditions with vibrational and rotational temperatures reaching several thousand Kelvin.[7] The gas-phase and surface reactions and energy transfer at these temperatures are essentially uncharacterized and the experimental methodologies capable of probing them are not well established. Under such circumstances, validated computational investigations become a valuable complementary tool.

In the present work, the formation of NO_2 from NO($^2\Pi$) and O(^{3}P) and its subsequent dissociation into oxygen-exchange and O_2 formation channels is investigated. Characterizing the kinetics and dynamics of a chemical reaction from computation usually requires a potential energy surface (PES) for the interactions involved. Within the framework of Molecular Dynamics (MD) simulations, this can either be an *ab initio*/semiempirical MD (AIMD) approach, a model PES or a parameterized, multidimensional PES fitted to electronic structure calculations, experimental observables, or a combination of the two.[8] Using AIMD is usually only possible for small systems and sufficiently short simulation times due to the considerable computational cost.[9–11] For parametrized PESs, the selection of the grid points on which the *ab initio* calculations are carried out is always a compromise between the computational cost and the intended purpose of covering the most significant regions of the configuration space (which is *a priori* unknown). A more efficient approach is to use separate grids for the different regions of interest and join them smoothly. In the asymptotic regions, that is, reactants or products, the dynamics is carried out on a single and simpler PES leading to a faster simulation. In the intermediate regions, the global surface is represented as a weighted sum of the contributions of all individual PESs. This approach has been successfully applied to connect different force fields.[12] We will

a)Present address: Institute of Materials and Environmental Chemistry, MTA Research Centre for Natural Sciences, Budapest, Hungary, Magyar tudósok körútja 2, Budapest, 1117 Hungary.
b)Author to whom correspondence should be addressed. Electronic mail: m.meuwly@unibas.ch.

pursue a similar strategy in the present work to build a global PES for NO_2.

A global PES for the 1^2A_1 and 1^2B_2 electronic states of NO_2 based on high-level *ab initio* calculations has been computed some years ago.[13] Very good agreement with the experimental results for the dissociation energies[14] and the equilibrium geometries was obtained from this PES.[15] The resulting frequencies calculated using filter diagonalization reasonably matched the experiments and values simulated from other published PESs. Both PESs in Ref. 13 were represented with three-dimensional cubic splines. In subsequent work, the long-range part of the 1^2A_1 PES and the lowest $1^2A''$ PES were corrected by considering the NO potential energy curve as a separate term in the PES at large NO–O separations. With this modification, the modeling of the collision dynamics to study the exchange and recombination reactions in O+NO collisions was performed.[16] For temperatures between 100 and 2500 K, the recombination (k_∞^r) and exchange rate coefficients (k_∞^{ex}) varied slightly within a factor of 2.[17]

The aim of the present work is the characterization of the reaction between $O(^3P)$ and $NO(^2\Pi)$ at higher temperatures relevant to the hypersonic flight regime of reentering spacecrafts. At a more fundamental level, we are particularly interested in establishing an efficient computational framework capable of probing small molecular systems for a wide range of parameters. The general approach is: (1) the construction of PESs for the ground state of the NO_2 molecule based on high-level *ab initio* calculations and their representation with a reproducing kernel Hilbert space (RKHS) method combined with Legendre polynomials; (2) quasi-classical trajectory calculations to study the adiabatic reaction dynamics, and (3) calculation of the rate coefficients for the different exit channels using a Monte Carlo method. The results of the simulations will be compared with previous computations[16–18] and experiments[13] in order to validate the computational approach. In the context of the hypersonic flight regime, the O_2 production channel ($NO+O \rightarrow O_2+N$) is of particular interest since the thermal dissociation threshold for O_2 is lower than that for N_2 in air. A central question is how translational excitation of the reactants and vibrational excitations of the NO affect the rate coefficient of O_2 formation.

A major focus here is to test and implement a computational protocol which should be suitable for routine and largely automated procedures in determining important fundamental inputs for reaction networks relevant to atmospheric and astrophysical modeling. The characterization of more complex chemical systems involves the modeling of a collection of reactions which can be arranged in a reaction mechanism where multiple elementary reactions take place at a wide range of changing conditions such as temperature and pressure.[19–24] In most cases, chemical processes in these networks occur out of equilibrium. This complicated panorama makes difficult the possibility of carrying out experiments nowadays. Even in implementing large scale simulations, a significant amount of data as input is required, for instance, the rate coefficients of the elementary reactions. This information may come from different sources either theoretical or experimental and it happens frequently that important data are not available. Given this scenario, the search for efficient computational frameworks for the calculation of the rate coefficients is an issue of primary interest.

The outline of the present work is as follows. In Sec. II, the methodology for constructing the PESs, the trajectory calculations, and the computation of the thermal quantities is discussed. Section III presents and discusses the results and in Sec. IV, conclusions about the validity of the approach are drawn.

II. METHODOLOGY

A. *Ab initio* calculations

The present calculations use Dunning's standard correlation-consistent polarized quadruple (cc-pVQZ) basis set, which is sufficiently large to properly describe the N–O and O–O bonds.[25,26] For a meaningful description of the geometries and energetics of the NO_2 molecule, its dissociation energetics and the conical intersections between the ground and the low-lying excited states, a multiconfigurational method is required. For this, the complete active space self-consistent field (CASSCF)[27] method is employed which takes into account static correlation. For recovering the dynamic correlation, e.g., during bond breaking and formation, multireference configuration interaction (MRCI) is used. The Davidson correction[28,29] is included to estimate the effects of higher excitations (MRCI+Q). All calculations are performed with the MOLPRO program ver. 2012.1.[30]

Figure 1 gives a schematic representation of the general relevant stages of the reaction of interest. NO_2 formation has a barrier of 1.3 eV from the N+O1O2 side, whereas from the NO1+O2 side it is a barrierless process. Initially, the $O(^3P)$ atom approaches the $NO(^2\Pi)$ molecule. Depending on the impact parameter b, the quantum state of the NO (vibrational and rotational) and the collision energy, the NO_2 molecule is formed. In the absence of additional collisional partners (zero pressure), the NO_2 will decay as it was formed with an energy above its dissociation limit. The following possibilities exist for the products: NO_2 can (1) dissociate into the same incoming constituents (NO1+O2 → NO1+O2), (2) dissociate into the same constituents but with the oxygen atoms exchanged (NO1+O2 → NO2+O1), (3) form dioxygen (O_2+N), or (4) atomize into the individual atoms (N+O1+O2).

In the presence of additional collisional partners, the NO_2 can loose its excess energy and stabilize. In the high-pressure

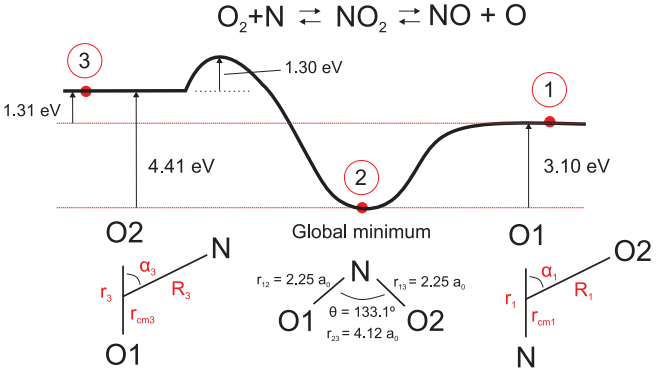

FIG. 1. Relevant stages in the NO1+O2 reaction. The energies were derived from the *ab initio* calculations of this work.

limit, this occurs for all trajectories which enter the potential well of NO_2 and thereby it is straightforward to determine the high-pressure limit rate coefficient for NO_2 formation.

In order to describe the different channels, three grids in Jacobi coordinates are employed to systematically cover the relevant regions of the PES for NO_2 (Figure 1). The first grid (for the NO1+O2 asymptote) includes the coordinates r_1 (the N–O1 distance), R_1 (the distance from the center of mass of NO1 to the oxygen atom O2), and α_1 (the angle formed by O1, the center of mass of NO1 and O2 (Figure 1)). With this grid, the entrance (NO1+O2) and NO_2-formation channels can be described. For the oxygen exchange channel (NO2–O1), a permutation of the oxygens in the first grid is performed. As a result, the second grid is defined by r_2, R_2, and α_2. For the third grid (O1O2+N), r_3 is the O–O distance, R_3 is the distance from the center of mass of the O_2 molecule to the nitrogen atom, and α_3 is the angle between O2, the center of mass of the O_2 molecule, and the nitrogen atom (Figure 1).

For the r_1 and r_3 coordinates, 12 points ($n_r = 12$) from 1.7 to 2.55 a_0 were selected. These points include the equilibrium positions and the turning points of the first four vibrational levels of the NO and O_2 molecules, respectively. Three additional points were used for a better description of the ground-state PES wells of the NO and O_2 molecules. The turning points for the NO molecule were those of a spectroscopically accurate Rydberg-Klein-Rees potential.[31,32] For the O_2 molecule, the turning points were obtained from the solution of the Schrödinger equation for a Morse potential fitted to density functional theory data.[33] As for the R_1 and R_3 coordinates, 29 points ($n_R = 29$) between 1.85 and 18.9 a_0 were selected. The α_1 and α_3 angles (in degrees) are from an 11-point ($n_\alpha = 11$) Gauss-Legendre quadrature ($\alpha = 11.98, 27.49, 43.10, 58.73, 74.36, 90.0, 105.64, 121.28, 136.9, 152.5, 168.02$). In total, 3828 points were calculated for each grid.

B. Representation of the PESs

In order to obtain a continuous PES for the NO_2 molecule from the reference *ab initio* calculations, a RKHS ansatz[34] (see below) for the distances (r and R) is combined with Legendre polynomials for the angles (α) (see Figure 1). First, for each combination (R,α), a set of functions $V_{R,\alpha}(r)$ is obtained by using a RKHS. In a second step, since the *ab initio* calculations were carried out at Gauss-Legendre points, the 2d-PES $W(R, \alpha)$ can be expanded in terms of Legendre polynomials $P_\lambda(\cos\alpha)$ as follows:

$$W(R, \alpha) = \sum_{\lambda=0}^{10} f_\lambda(R) P_\lambda(\cos\alpha), \tag{1}$$

where $f_\lambda(R)$ are radial coefficients ("radial strength functions")[35] and λ is their order. A second RKHS interpolation is then used along the R-coordinate.

The energy at an off-grid point (r', R', and α') is evaluated as follows. From the direct evaluation of the functions $V_{R,\alpha}(r)$ at r', a set of energies, $W(R, \alpha; r')$ for each combination of (R, α) on the grid is obtained which yields a 2-dimensional PES. By expanding $W(R, \alpha; r')$ in Legendre polynomials up to order $\lambda_{\max} = 10$, the following $n_\alpha \times n_\alpha$ linear system is obtained:

$$\sum_{\lambda=0}^{n_\alpha - 1} f_\lambda(R_j) P_\lambda(\cos\alpha_k) = W(R_j, \alpha_k; r'), \tag{2}$$

where α_k, $k = 1, \ldots, (n_\alpha - 1)$, are the Gauss-Legendre points. Solving this linear system for $f_\lambda(R_j)$ on all n_R grid points R_j (see Eq. (2)) yields new radial strength functions which are represented as a RKHS. These kernels can be evaluated at position R'. Finally, evaluating Eq. (2) at $\alpha_k = \alpha'$ gives the energy $W(R', \alpha'; r')$ at an off-grid point. It should be emphasized that truncating the Legendre expansion at finite $\lambda_{\max}$ potentially leads to inaccuracies in regions where variations along α are appreciable. However, it is found that radial cuts along R for neighboring angles α_k show similar behaviours. An explicit comparison is provided in the inset of Figure 4. Based on this, retaining 11 terms in the angular degree of freedom was deemed sufficient.

Details about the RKHS procedure can be found in the literature.[34] Here, only the essentials are summarized for completeness. Within the RKHS framework, a multidimensional function $V(\mathbf{R})$ (here the PES) which depends on the molecular coordinates $\mathbf{R}$ is assumed to belong to a RKHS, that is, $V(\mathbf{R})$ is a bounded linear function. Thus, the function $V(\mathbf{R})$ can be represented as

$$V(\mathbf{R}) = \sum_{k=1}^{M} \alpha_k Q(\mathbf{R}_k, \mathbf{R}), \tag{3}$$

where $\mathbf{R} = (x'_1, \ldots, x'_F)$ indicates the F internal coordinates for a given nuclear configuration of the system, at which the interpolated energy is sought, $\mathbf{R}_k = (x_{k1}, \ldots, x_{kM})$ are the coordinates of the M *ab initio* energies, and $Q(\mathbf{R}_k, \mathbf{R})$ is the reproducing kernel which consists of a set of linearly independent functions also belonging to the RKHS. The α_k in Eq. (3) satisfy the relation

$$\sum_{l=1}^{M} Q_{kl}\alpha_l = V(\mathbf{R}_k), \qquad k = 1, 2, \ldots, M, \tag{4}$$

where $Q_{kl} = Q(\mathbf{R}_k, \mathbf{R}_l)$ and $V(\mathbf{R}_k)$ are the *ab initio* energies at the grid points (Figure 1). The α_l are determined once from a Cholesky decomposition.[36] The reproducing kernel, $Q(\mathbf{R}_k, \mathbf{R})$ for a multidimensional PES can be represented as a product over 1-dimensional kernels $q_i(x_{ki}, x'_i)$

$$Q(\mathbf{R}_k, \mathbf{R}) = \prod_{i=1}^{F} q_i(x_{ki}, x'_i). \tag{5}$$

For 1-dimensional distance-like variables, the following explicit expression for the kernel was employed:

$$q^{n,m}(x, x') = n^2 x_>^{-(m+1)} B(m+1, n) \times {}_2F_1\left(-n+1, m+1; n+m+1; \frac{x_<}{x_>}\right), \tag{6}$$

where $x_>$ and $x_<$ are the larger and the smaller of x and x', respectively, $B(m + 1, n)$ is the beta function, and ${}_2F_1(-n+1, m+1; n+m+1; \frac{x_<}{x_>})$ is the Gauss hypergeometric function.[37] The superscripts n and m are related to the smoothness of the function to be interpolated and the reciprocal power of the distance weighting factor, respectively. In

TABLE I. Spectroscopic constants for the ground state of NO and O_2 molecules.

NO molecule	Our calculations	Experiments (Ref. 33)
ω_e (cm^{-1})	1922.01	1904.1
$\omega_e x_e$ (cm^{-1})	14.48	14.09
O_2 molecule		
ω_e (cm^{-1})	1607.5	1580.2
$\omega_e x_e$ (cm^{-1})	14.1	12.0

the present work, $n = 2$ (smoothness criterion applied up to the first derivatives of the potential) and $m = 6$ which corresponds to a $1/x^6$ long-range interaction, although different dependencies could also be considered.[38]

The RKHS procedure is a generic and parameter-free method. It can be used for constructing n-dimensional PESs from either regular or irregular grids which is an additional advantage. The asymptotic behavior of the interactions can be explicitly taken into account (see above). If molecular symmetry is present, this can also be employed (e.g., permutational symmetry) and explicit analytical derivatives of the kernel are available. Because the long-range behavior can be controlled and analytical derivatives are available, a RKHS-based PES offers potential advantages over cubic (or higher-order) spline interpolations. A possible drawback of the RKHS method is the cost of the calculation of the α_λ in Eq. (4) which, however, needs to be done only once and the evaluation of the reproducing kernel $Q(\mathbf{R}_k, \mathbf{R})$ at every new calculation of the potential energy $V(\mathbf{R})$. This may not be a problem if the pre-summations of the method are handled in an efficient manner.[39]

To properly describe the asymptotic behavior of the PES for large separations between the reactants, Morse potentials ($V = D_e[1 - \exp(-\beta(r - r_e))]^2$) were fitted to the *ab initio* energies for the NO and O_2 monomers. The resulting parameters were $D_e = 7.91$ eV, $\beta = 1.34\ a_0^{-1}$, and $r_e = 2.17\ a_0$ for NO and $D_e = 5.67$ eV, $\beta = 1.37\ a_0^{-1}$, and $r_e = 2.29\ a_0$ for O_2. The reported spectroscopic data are $D_e = 6.623$ eV and $r_e = 2.18\ a_0$ for NO, and 5.21 eV and 2.28 a_0 for O_2, respectively.[33] The disagreement in the dissociation energies of NO (experimental and calculated) does not affect the results since the full atomization process is not considered here as explained further below. For further characterization of the NO and O_2 molecules, the spectroscopic constants calculated from the Morse potential parameters are compared to experiments in Table I.[40] The results indicate a better agreement for the anharmonic term ($\omega_e x_e$) for the NO molecule.

For the global PES for the system, the local PESs determined for the three grids corresponding to the relevant channels of the reaction (Figure 1) need to be joined. For this, the global PES is written as the weighted sum of the three asymptotic PESs

$$V(\mathbf{x}) = \sum_{j=1}^{3} w_j(\mathbf{x}) V_j(\mathbf{x}), \tag{7}$$

where $\mathbf{x} = (r_{12}, r_{13}, r_{23})$ are the three interatomic distances of the NO_2 molecule (Figure 1), and $V_1(\mathbf{x})$, $V_2(\mathbf{x})$, and $V_3(\mathbf{x})$ are the potential energies for the three regions for which the distances r_{12} (N–O1), r_{13} (N–O2), and r_{23} (O1–O2) are small, and the remaining distances vary from small to large, respectively. The weights $w_j(\mathbf{x})$ are coordinate-dependent and result from the normalization of the following weight functions:

$$w_{j0}(x_j) = \exp(-x_j/\Delta R), \tag{8}$$

$$w_j(x_j) = \frac{w_{j0}(x_j)}{\sum_{l=1}^{3} w_{l0}(x_l)}, \tag{9}$$

where x_j are either r_{12} or r_{13} or r_{23} and $\Delta R = 0.05\ a_0$. A similar weighting function was successfully used in Multisurface Adiabatic Reactive Molecular Dynamics (MS-ARMD) which uses the energy as the control parameter in connecting multiple force fields.[12]

C. Molecular dynamics simulations

1. Generation of the initial conditions

Armed with a globally valid PES, the dynamical evolution of the system is followed by propagating Hamilton's equations of motions subject to initial conditions. The equations of motion are integrated numerically using the Velocity-Verlet algorithm.[41] Since the total linear and angular momenta are conserved during the dynamics, it is convenient to select the center of mass of the NO_2 molecule as the origin of the coordinate system. In order to capture the fastest nuclear movements in the system, a time step of 2 a.u. (a.u. means atomic unit of time) (4.84×10^{-2} fs) was used for the propagation. Trajectories were started from an initial separation of (min(15 a_0, impact parameter + 5 a_0)) and followed until the fragments had separated to the same distances. If this criterion was not met, integration continued for a maximum time of the estimated interactionless time of flight (see below) through the "reaction-zone" plus an additional 100 ps, during which most of the NO_2 molecules decayed except for very few low-energy (low E_c and low rovibrational state of initial NO) trajectories.

Suitable initial conditions for NO were generated from a WKB[42]-quantized periodic orbit of the corresponding rotating Morse oscillator for given vibrational v and rotational j quantum numbers.[43] The symmetry axis of the NO molecule and the axis of its rotation, which are orthogonal to each other, was also randomly orientated as was the NO angular momentum. Sampling of the initial rovibrational quantum states of NO, the impact parameter (b) and the collision energy (E_c) are discussed in Sec. II D.

For characterizing the reaction at a given temperature, 4 different cases from I to IV are considered:

(I) corresponds to NO_2-formation in the high-pressure limit. The NO_2 molecule stabilizes through collisions with the environment. We will indicate this by "∞" as superscript ($k^\infty(T)$). For the formation of NO_2, the same criterion as in Ref. 16 is assumed, that is, the oxygen atom O2 is captured once it approaches to within less than 3.78 a_0 of the center of mass of NO1.

(II) is for NO_2 formation and survival which carries the label "NO_2" as superscript ($k^{NO_2}(T)$). For this case, the

"oxygen capture criterion" (see item (I)) is combined with a lifetime criterion, defined as $t_{life} = t_{traj} - t_{tof} > 0$. Here, t_{traj} is the total time of the trajectory, which is either (a) $t_{traj} = 100$ ps for the case that NO_2 does not dissociate or (b) the time until any of the interatomic separations is larger than the initial separation of NO1–O2. The interactionless time of flight $t_{tof} = 2\sqrt{(R_{ini}^2 - b^2)}/v_{ini}$ is determined from the initial conditions.

(III) is the oxygen atom exchange reaction, "ex" with associated rate coefficient $k^{ex}(T)$. The criterion for this case is that the N–O2 distance is small and the N–O1 or O1–O2 distances are large.

(IV) refers to oxygen molecule formation (O1O2+N) and the corresponding rate coefficient is $k^{O_2+N}(T)$. This case is encountered if the O1–O2 distance is small and the N–O1 or N–O2 distances are large.

An additional possible process is full atomization into N+O+O. However, this channel is not considered because even at $T = 20\,000$ K, when the NO_2 complex potentially contains sufficient energy for atomization, the probability to decay through this channel is small. This is based on considering the probability distributions for the rovibrational energy of the NO and O_2 molecules in the product channels and the following reasoning.

First, direct three-body breakup is extremely unlikely which only leaves dissociation into an atom plus diatom system. After breakup a considerable amount of energy is in the relative translation of the atom + diatom products. Dissociation of the diatomic occurs whenever the vibrational energy (on the effective potential) exceeds the dissociation energy level of the diatomic molecule. When the rotational quantum number j of the product diatomics is smaller than $j = 50$ (see inset in Figure 2), the effect of rotation on decreasing the dissociation energy via centrifugal forces will be insignificant. Figure 2 reports the rovibrational energy distributions for NO and O_2. They indicate that the probability for NO-dissociation is very small whereas dissociation of O_2 is more likely (about 20%). However, this occurs still with very low probability since the centrifugal barrier of the rotating diatomics does not allow the molecule to dissociate in a classical simulation, even if its energy is larger than the asymptotic energy level for decomposition but still less than the top of the centrifugal barrier. This explains why fewer dissociation events are found than expected based on energetics alone and is confirmed in the simulation. Only 63 out of the 10 000 trajectories end up in N+O+O and all of them take place via O_2 dissociation. The implication is that dissociation into either the O_2 or NO channels is fast and the final fragmentation to the fully atomic channel is slow. Therefore, the atomic channel will not affect the rate coefficients of the diatomic channels.

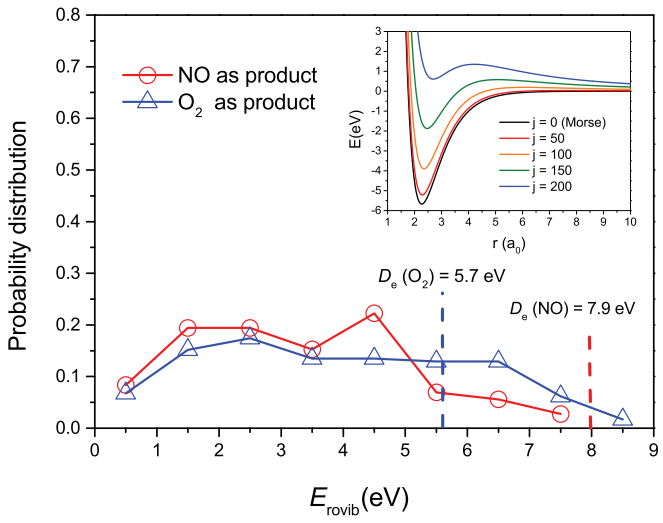

FIG. 2. Probability distributions of the rovibrational energy for NO and O_2 molecules in the products at 20 000 K are shown separately. The blue and red vertical dashed lines are the calculated dissociation energies for O_2 and NO, respectively. The corresponding experimental values are 6.62 eV and 5.21 eV for NO and O_2, respectively. The inset in the figure shows the effective potential of the O_2 molecule ($V^{Morse}(r) + j(j+1)\hbar^2/2\mu r^2$, where μ is the reduced mass between the oxygen atoms and r the interatomic distance) for $j = 0$, 50, 100, 150, and 200.

D. Monte Carlo calculation of the thermal rate coefficients

The thermal rate coefficient[44–46] can be determined from

$$k(T_t, T_{rv}, T_e) = \frac{\beta_t}{g(T_e)}\sqrt{\frac{8\beta_t}{\pi\mu}} \int_0^\infty \sigma(E_c; T_{rv}) E_c e^{-\beta_t E_c} dE_c, \tag{10}$$

where $\beta_t = k_B T_t$ and k_B is the Boltzmann constant, T_t, T_{rv}, T_e are the translational temperature of NO and O, the rovibrational temperature of NO and the electronic temperature of NO, respectively, $g(T_e)$ is the electronic degeneracy factor,[17,47] μ is the reduced mass of NO1 and O_2, respectively, and $\sigma(E_c; T_{rv})$ is the integral cross section as a function of the collision energy, E_c and T_{rv}. In our studies, it was assumed that $T_t = T_{rv} = T_e$. In other words, the various degrees of freedom in the reactants are in thermal equilibrium. If no subscript is shown for T, then it corresponds to the common temperature. In a similar manner, the reaction cross section $\sigma(E_c; T_{rv})$ for a given collision energy E_c is

$$\sigma(E_c; T_{rv}) = \frac{\sum_{v=0}^{v_{max}} \sum_{j=0}^{j_{max}(v)} (2j+1) e^{-\beta_{rv} E_{vj}} \sigma_{vj}(E_c; vj)}{\sum_{v=0}^{v_{max}} \sum_{j=0}^{j_{max}(v)} (2j+1) e^{-\beta_{rv} E_{vj}}}, \tag{11}$$

where $\sigma_{vj}(E_c)$ is the (v, j)-state dependent cross section at collision energy E_c. The energy E_{vj} of a rovibrational state (v, j) is calculated according to a Morse oscillator model for the NO molecule.[43] The cross section as an integral of the opacity function $P_{vj}(b; E_c)$ for given E_c and rovibrational state (v, j) is

$$\sigma_{vj}(E_c) = \int_0^\infty P_{vj}(b; E_c) 2\pi b db. \tag{12}$$

Assuming a thermal distribution of the reactants $O(^3P)$ and $NO(^2\Pi)$ the expression for the electronic degeneracy

factor, $g(T_e)$[17,47] is

$$g(T_e) = [5 + 3\exp(-227.8\,\mathrm{K}/T_e) + \exp(-326.6\,\mathrm{K}/T_e)] \times [1 + \exp(-177.1\,\mathrm{K}/T_e)]. \quad (13)$$

The integral in Eq. (10) can be calculated by using an Importance Sampling Monte Carlo scheme.[48] For this, the vibrational and rotational quantum numbers v and j, and the collision energy (E_c) are sampled from the following probability distributions:

$$p_{vj}(T_{rv}) = \frac{(2j+1)e^{-\beta_{rv}E_{vj}}}{\sum_{v'=0}^{v_{max}}\sum_{j'=0}^{j_{max}(v')}(2j'+1)e^{-\beta_{rv}E_{v'j'}}}, \quad (14)$$

and

$$\rho(E_c)\mathrm{d}E_c = \beta_t^2 E_c e^{-\beta_t E_c}\mathrm{d}E_c, \quad (15)$$

respectively.

For the determination of the upper limit (b_{max}) of the relevant sampling interval for the impact parameter, b, preliminary tests were carried out at low temperatures (100 and 200 K). As NO_2 was not formed for $b \geq 26\ a_0$, the impact parameter was uniformly sampled from 0 up to $b_{max} = 26\ a_0$.

After evaluating the integral in Eq. (10) over v, j, and E_c, the resulting expression for $k(T)$ is

$$k(T) = \sqrt{\frac{8}{\pi\mu\beta}}\frac{2\pi b_{max}}{g(T)N_{tot}}\sum_{i=1}^{N_{reac}} b_i, \quad (16)$$

where N_{reac} and N_{tot} are the number of reactive and the total number of trajectories, respectively, and b_i is the impact parameter of reactive trajectory i. The convergence of the integral in Eq. (10) was monitored by the decrease of the Monte Carlo error.

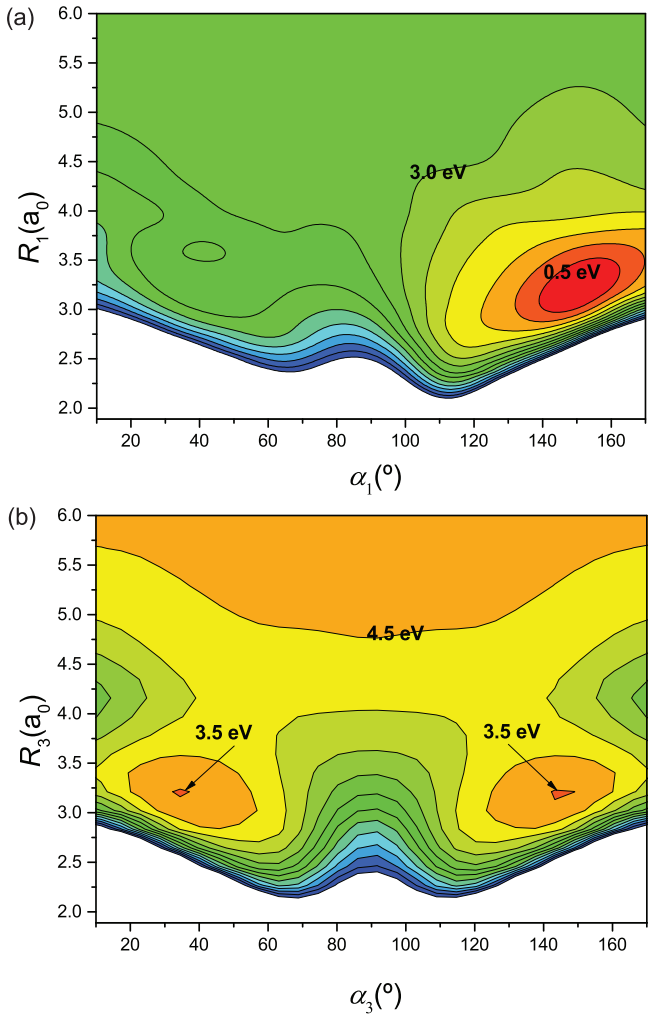

FIG. 3. Contour plots for the NO1+O2 (panel (a)) and O2O1+N (panel (b)) grids in R_1, α_1 and R_3, α_3 Jacobi coordinates, respectively. The N–O1 (r_1) and O2–O1 (r_3) distances were set to 2.25 a_0. In both cases, the contour levels are separated by 0.5 eV.

III. RESULTS AND DISCUSSION

A. The ground state $1^2A'$ PES

In the present work, the reaction dynamics of NO_2 on the ground-state ($1^2A'$) PES is considered. Even when the excited states can approach the ground state PES for certain configurations (see Figure 1 in the supplementary material[49]), their influence can be considered to be minor as it requires 6 eV to access them. According to the Maxwell-Boltzmann distribution for 20 000 K, translational energies beyond 6 eV are accessed with little probability (0.06). This is further decreased if one takes into account that some energy goes into rotational and vibrational states of NO which are distributed according to the Boltzmann distribution before the reaction takes place. Furthermore, lifetimes of the excited states are smaller the higher the rovibrational energy. This causes the system to rapidly return to the ground state.[17] The expected effect of including the excited states in the dynamics would be a slight lowering of the reaction rate coefficients. Therefore, in this work we first consider only the ground state PES since it dominates the reaction dynamics under the relevant physicochemical conditions.

The smoothness of the RKHS interpolation is evident in the contour plots of Figure 3. In panel (a), the PES for the "NO1+O2" channel is shown. The global minimum was found at $R_1 = 3.21\ a_0$ and $\alpha_1 = 150.8°$ ($r_{NO} = 2.25\ a_0$ and $\theta_{O\text{–}N\text{–}O} = 133.1°$ (Table II) in internal coordinates). The PES for the "O1O2+N" channel is reported in panel (b). Two symmetric minima are observed for the same R_3 Jacobi distance which is measured from the center of mass of O_2 to the N atom.

In order to assess the quality of the interpolated RKHS PES, an additional (off-grid) cut for $r = 1.21$ Å (N–O1 distance) and $\alpha = 34°$ was calculated along the R-coordinate at the MRCI+Q/cc-pVQZ level. The comparison between the computed *ab initio* energies and those from the 3d-interpolant is reported in Figure 4. The average mean difference over the entire range is 0.03 eV (see inset in Figure 4). The cuts for two Gauss-Legendre quadrature angles, that is ($\alpha = 27.5$ (open squares) and 43.1° (open triangles)), are also included in order to show that by construction, the RKHS curves go through the *ab initio* energies.

TABLE II. Equilibrium geometries and normal mode frequencies from the present work and from Ref. 13 and experiments. The variables $r_{1,e} = r_{2,e}$, $\theta_{O\text{–}N\text{–}O}$, and D_e are the equilibrium N–O distance, the O–N–O angle, and the well depth for the global minimum of NO_2, respectively.

Equilibrium NO_2	Present work	Ref. 13	Experiments
$r_{1,e} = r_{2,e}$ (a_0)	2.25	2.26	2.255[15]
$\theta_{O\text{–}N\text{–}O}$ (deg)	133.1	134.3	133.9[15]
D_e (eV)	3.21	3.11	3.23[14,51,52]
Normal frequencies (cm^{-1})			
Symmetric stretch	1322.7	1333.6	1319.794[50]
Asymmetric stretch	1623.3	1658.0	1616.852[50]
Bending mode	759.6	755.0	749.649[50]

Some features of the present ground state PES are summarized in Table II and compared to results from previous calculations[13] (using icMRCI+Q/cc-pVQZ with CASSCF(13,10)) and to experiments[14,15,50–52] (high-resolution microwave spectroscopy[15] and laser induced fluorescence[51]). Good agreement with previous computations and experiments was found from the methods used in the present work.

B. Thermal rate coefficients

A total of 10 000 individual trajectories was run at each temperature, including $T = 100$, 200, 300, 400, 1000, 1500, 2000, 2700, 5000, 7000, 10 000, 15 000, and 20 000 K. In the following, the thermal rate coefficients obtained from the trajectory calculations are presented. The convergence of the computed rate coefficient is reported in Figures 5(a) and 5(b). In panel (a), the thermal rate coefficient for NO_2 formation in the high-pressure limit, $k^\infty(T)$, is shown as a function of the number of trajectories for $T = 10\,000$ K. The relative error ($(2\sigma_S/k^\infty)100\%$, where σ_S is the standard deviation) decreases to ≈2.5% if all 10 000 trajectories are used to compute $k^\infty(T)$. In panel (b), the decrease of the relative error with the number of trajectories is shown for selected temperatures. The horizontal line indicates 10% of the relative error for which ≈600 trajectories are required. This indicates that the computational strategy is very efficient in exploring the relevant regions of the initial phase-space for the thermal rate coefficient calculations.

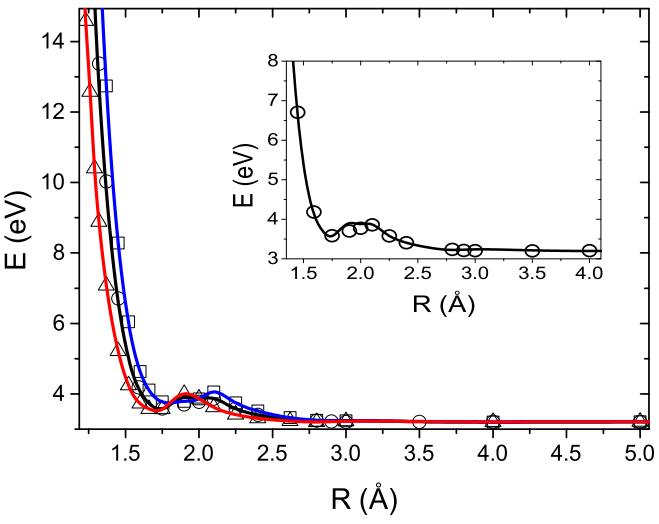

FIG. 4. MRCI+Q/cc-pVQZ energies along the R coordinate for $r = 1.21$ A (N–O1 distance) and $\alpha = 27.5°$, 34.0°, and 43.1° (open squares, open circles, and open triangles, respectively). R, r, and α are Jacobi coordinates. The solid lines are RKHS interpolants. The inset in the graph represents a close-up of the cut for $\alpha = 34.0°$ which is not a Gauss-Legendre quadrature angle.

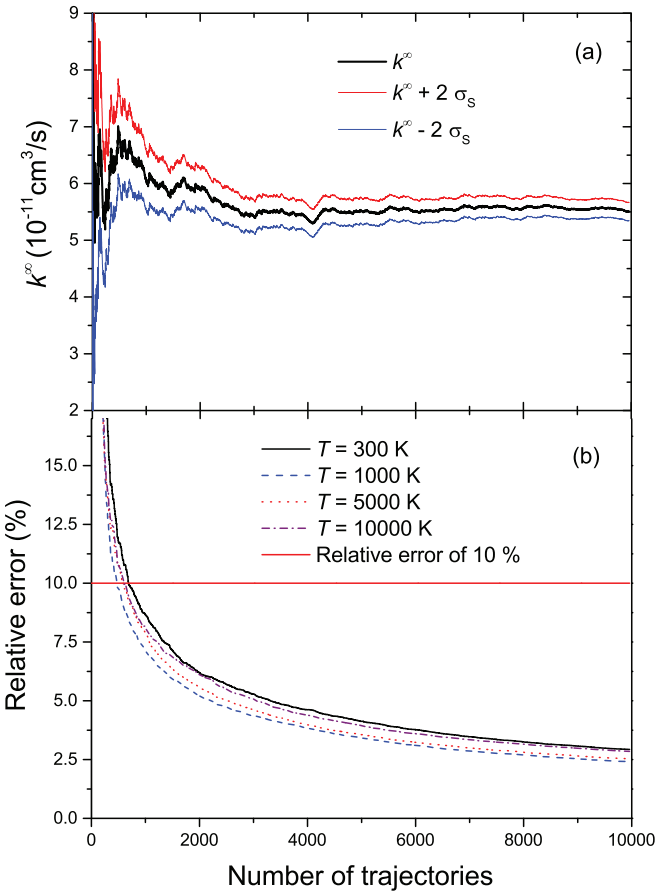

FIG. 5. Convergence of the Monte Carlo integral for the thermal rate coefficients for NO_2 formation in the high-pressure limit at $T = 10\,000$ K *versus* the number of trajectories (panel (a)). The confidence interval corresponds to two times the standard deviation (σ_S). In panel (b), the relative error as a function of the number of trajectories is reported for $T = 300$ K (solid), 1000 K (dashed line), 5000 K (dotted line), and 10 000 K (dashed-dotted line). The red horizontal line indicates a relative error of 10%.

In Figure 6, the thermal rate coefficients for NO_2 formation in the high-pressure limit, $k^\infty(T)$, are shown and compared with published computational and experimental results. Even though the major interest here concerns the high-temperature range, these data provide a validation of the computational procedure put forward in the present work. We report the error bar as twice the standard deviation (σ_S) in order to include 95.4% of the cases in the confidence interval. In the following, it is important to emphasize that the present results are from simulations using the $1^2A'$ PES only (open squares with solid line). The present results are in reasonable agreement with results from previous calculations[17] (solid down-oriented triangles) which also used the $1^2A'$ PES only, although with a different parametrization. Both calculations underestimate the experimentally determined thermal rate

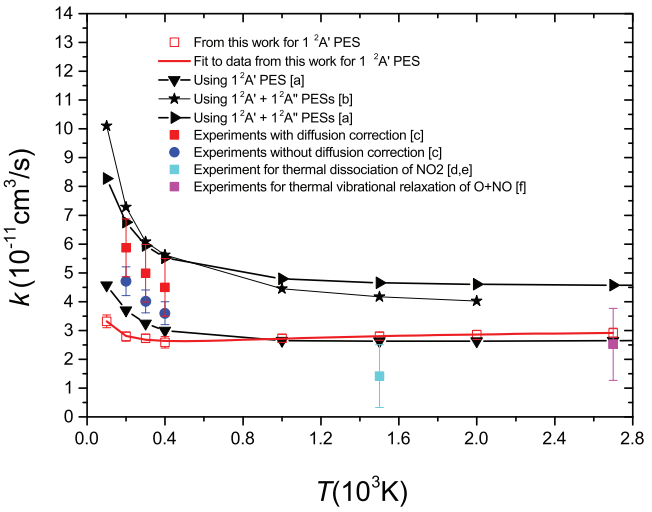

FIG. 6. Thermal rate coefficients for the NO_2 formation in the high-pressure limit, $k^{\infty}(T)$ *versus* temperature. In the legend, [a] = Ref. 17, [b] = Ref. 16, [c] = Ref. 18, [d] = Ref. 53, [e] = Ref. 54, and [f] = Ref. 58.

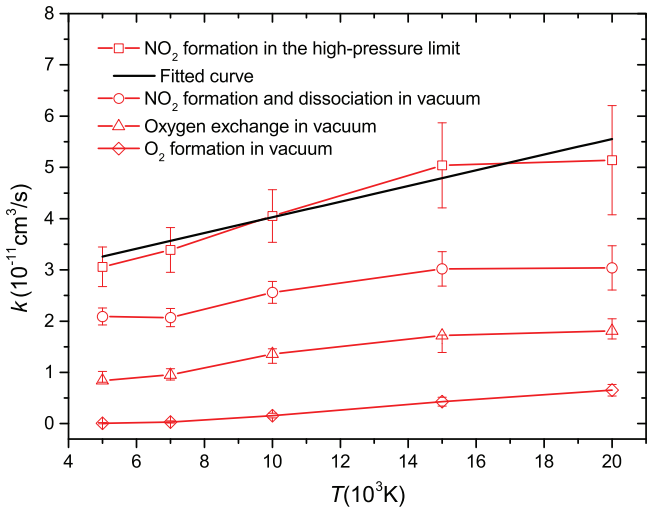

FIG. 7. High-pressure limit thermal rate coefficients for NO_2 formation (squares) (fit with black solid line), NO_2 formation and dissociation (circles), oxygen exchange channel (up-oriented triangles), and oxygen production channel (diamonds).

coefficients at $T = 200$, 300, and 400 K (solid circles and squares). At 2700 K, the computed rate coefficient compares favourably with experimental data.[53,54]

No correction was made for zero-point energy (ZPE) and other quantum effects, such as tunneling through the centrifugal barrier which can be still significant at low temperatures. The centrifugal barrier originates from the conservation of the total angular momentum and consists of the rotational energy associated with the orbital angular momentum of the colliding partner with respect to the center of mass of the whole system. The orbital angular momentum is directly proportional to the impact parameter and with the initial relative momentum of reactants. An increase of the thermal rate coefficient for lower temperatures has been found to be related to tunneling through the entrance barrier in the reaction of OH with methanol ($T < 200$ K) and O(^{3}P) with alkenes ($T \sim 20$ K).[55,56] This has also been shown in theoretical studies of HCOH isomerizations.[57] On the other hand, results when using the two lowest $1^2A'$ and $1^2A''$ PESs indicate that the $1^2A''$ PES might play an important role along with quantum effects at temperatures below 400 K. However, for temperatures above 1000 K the results using only the $1^2A'$ PES reasonably match with the experimental results, e.g., for 1500 and 2700 K. This can be explained by noting that the well of the electronically excited C-state of NO_2 (C $1^2A''$) is comparatively small and leads to redissociation of NO_2 at high temperatures.[17] Given this, the influence of tunneling and the $1^2A''$ PES at high temperature appear to be negligible.

For practical work in reaction networks,[19] it is advantageous to use a parametrized form for $k^{\infty}(T)$. A previously considered empirical expression[17] has been fitted to the results from simulations using the $1^2A'$ PES,

$$k^{\infty}(T)/(10^{-11}\mathrm{cm}^3/\mathrm{s}) = 2.715 + 0.4490 \ln T/\mathrm{K} + 0.3385\,(\ln T/\mathrm{K})^2 - 0.7134\,(\ln T/\mathrm{K})^3. \quad (17)$$

This yields the red solid line in Figure 6.

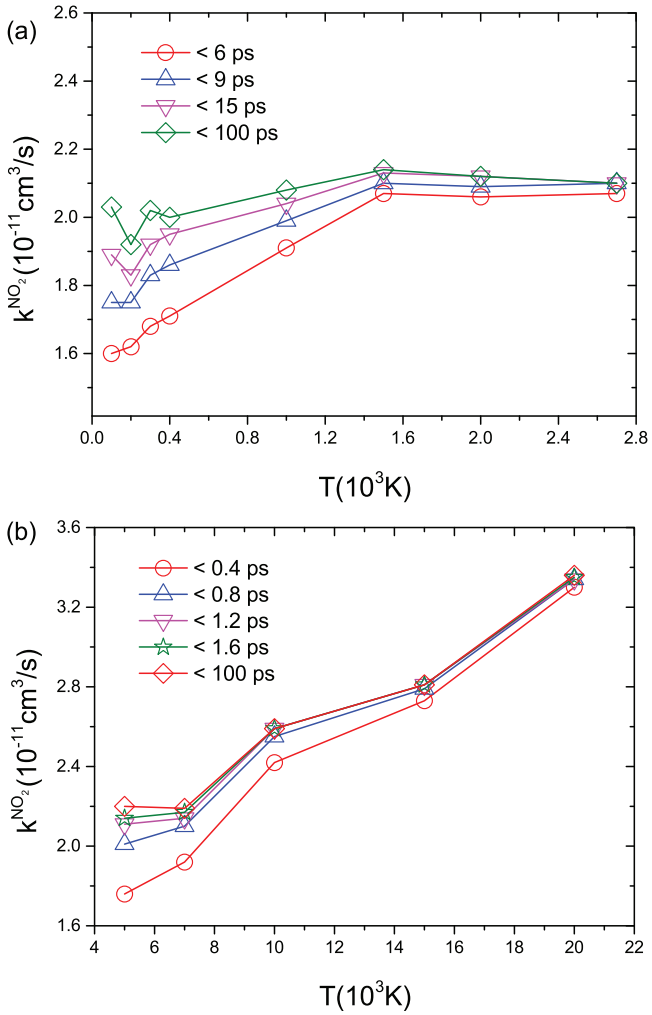

FIG. 8. Thermal reaction rate coefficients for NO_2 formation and decay, $k^{NO_2}(T)$ for different thresholds of the lifetime. Results for lower temperatures (100-2700 K) are shown in panel (a) and for higher temperatures (5000-20 000 K) in panel (b).

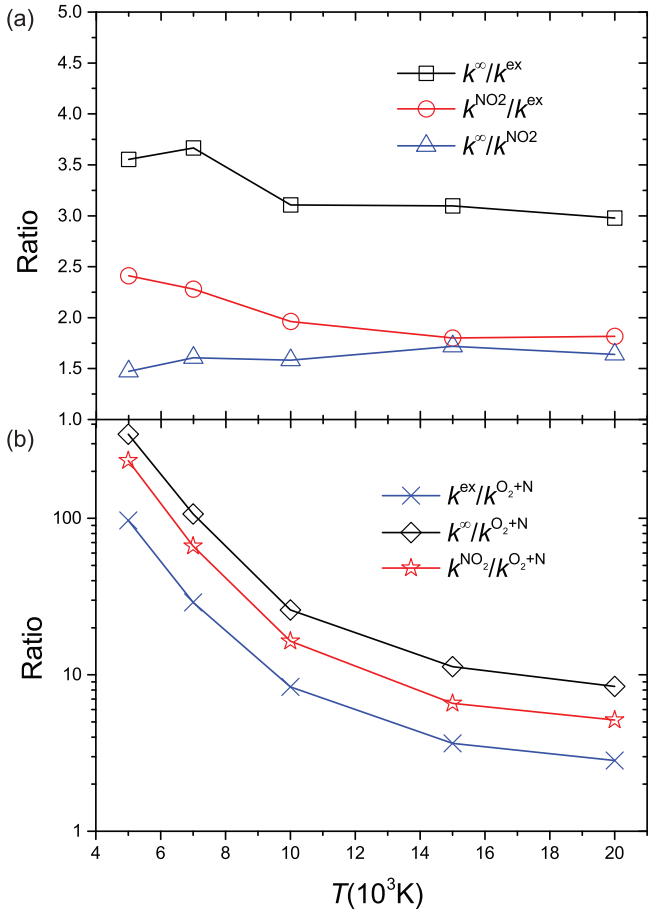

FIG. 9. (a) and (b) Ratios of the rate coefficients of different channels.

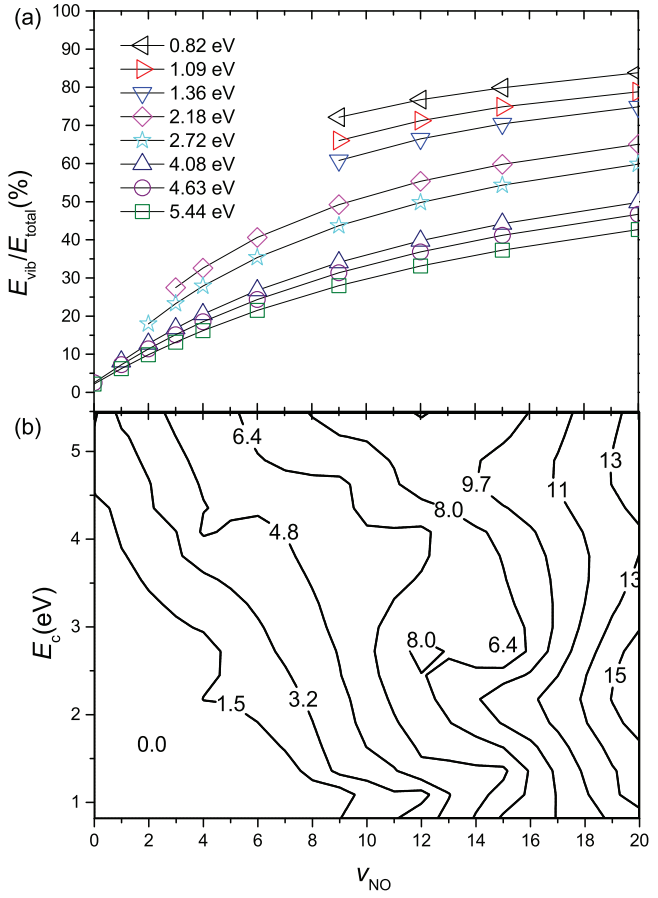

FIG. 10. Fraction of initial vibrational energy of NO with respect to the total energy *versus* the vibrational quantum number for 8 values of the collision energy (panel (a)). The contour plot of the channel probability as percentage is shown in panel (b). Only data for "O_2+N" channel are shown.

The thermal rate coefficients for temperatures between $T = 5000$ K and $T = 20\,000$ K are reported in Figure 7 for cases I-IV studied in this work. With increasing temperature a slight increase in the thermal rate coefficients is found. At 20 000 K, they increase to $k^{\infty} = 5.5 \times 10^{-11}$ cm^3/s, $k^{NO_2} = 3.4 \times 10^{-11}$ cm^3/s, $k^{ex} = 1.9 \times 10^{-11}$ cm^3/s, and $k^{O_2+N} = 0.65 \times 10^{-11}$ cm^3/s. Again, for practical purposes the data for $k^{\infty}(T)$ were fitted to a linear equation as (solid line in Figure 7)

$$k^{\infty}(T)/(10^{-11}\text{cm}^3/\text{s}) = 2.497 + 0.1529(T/\text{K}). \quad (18)$$

Figure 8 reports the rate coefficient for NO_2 formation and decay, $k^{NO_2}(T)$, for different thresholds for the lifetime of the NO_2 molecule. Panel (a) shows results for lower temperatures (100-2700 K) and panel (b) those for higher temperatures (5000-20 000 K). The results indicate that the NO_2 molecule lifetimes (see definition of lifetime (t_{life}) in Sec. II) are mostly below 16 ps and 1.6 ps for low and high temperatures, respectively.

In order to identify which process is relevant at higher temperatures, the ratios between the thermal rate coefficients are shown in Figures 9(a) and 9(b) for the different cases. In all cases, the ratios become almost constant at higher temperatures. The values for 20 000 K are: $k^{\infty}/k^{ex} \approx 3$, $k^{NO_2}/k^{ex} \approx 1.8$, $k^{\infty}/k^{NO_2} \approx 1.6$, $k^{\infty}/k^{O_2+N} \approx 8.4$, $k^{NO_2}/k^{O_2+N} \approx 5.2$, and $k^{ex}/k^{O_2+N} \approx 2.8$. At this temperature, the oxygen exchange channel is about 3 times faster than the "O_2+N" channel.

For a more detailed description of the O_2 production channel, Figure 10 (panel (a)) reports the fraction of initial vibrational energy of NO relative to the total energy *versus* the vibrational quantum number of NO (v_{NO}) for 8 values of the collision energy. The fraction of collision energy is complementary to the vibrational energy to give the total energy of the system ($E_c + E_{vib} = E_{tot}$). In panel (b), the contour plot of the channel probability is shown. In all cases, the rotational ground state ($j_{NO} = 0$) is assumed. For this calculation, 2500 trajectories were run for each combination of $E_c = \{0.82, 1.09, 1.36, 2.18, 2.72, 4.08, 4.63, 5.44\}$ eV and $v_{NO} = \{0, 1, 2, 3, 4, 6, 9, 12, 15, 20\}$ values. The results indicate that for $v_{NO} = 0$ the O_2-channel opens only for very high collision energies (>4.63 eV). However, for an initial NO-state with $v_{NO} = 9$ (corresponding to $E_c = 0.82$ eV) production of 0.6% of O_2 is observed. This qualitatively follows from Polanyi's rule[44] which predicts that the reaction should go to the late-barrier "O_2 + N" channel when the NO molecule is initially vibrationally highly excited even for low collisional energies. In order to give a clearer picture of this, the reaction is considered to start from N+O_2 (left side in Figure 1). In this situation, the reactants experience an early barrier of about 1.3 eV (Figures 1 and 3(b)). The exit channel in this case

is barrierless (NO1 + O2). According to Polanyi's rule, the excess energy released after crossing the early barrier goes predominantly into the internal degrees of freedom in the products (NO1) rather than into their (relative) translational energy.

For the set of vibrational quantum numbers and energies studied, the maximum channel probability of 13% for O_2-formation is reached at $v_{NO} = 20$. In general, the trend indicates that for lower vibrational quantum numbers, more energy needs to be in the translational degree of freedom. Conversely, for higher vibrational excitation of the NO, less collision energy is required. When both the collision energy and the vibrational quantum number of NO are high, the reaction probability of $N+O_2$ formation is maximal.

IV. CONCLUSIONS

The $O(^3P) + NO(^2\Pi)$ reaction has been studied over a range of temperatures relevant for the hypersonic flight regime (5000-20 000 K). For this purpose, the thermal cross sections and rate coefficients were calculated for the different exit channels. The results indicate that oxygen exchange (NO2+O1) occurs at all temperatures. However, O_2-formation is only found for $T \geq 5000$ K. For both channels, the thermal rate coefficient increases as the temperature increases ($T = 5000$-20 000 K). A more detailed scrutiny of the "O1O2+N" channel indicates that the smaller the vibrational quantum number of NO, the higher translational energy is required to open it; conversely, the higher the vibrational quantum number, the less translational energy is needed. Our results for lower temperatures are discussed and compared to previous experimental and computational results. In this respect, this work also presents the validation of an efficient computational protocol for the investigation of reaction dynamics of triatomic systems. Two aspects make the approach efficient and accurate. First, the *ab initio* energies are handled by means of a RKHS representation which is accurate, computationally convenient, and correctly describes the asymptotic regions of the PESs. Second, thermal quantities are calculated by using Importance Sampling which is efficient to evaluate multi-dimensional integrals over the phase-space of initial states. With less than 1000 classical trajectories a relative error below 10% for the rate coefficients is obtained.

ACKNOWLEDGMENTS

Part of this work was supported by the United States Department of the Air Force which is gratefully acknowledged (to J.C.C.P.). Support by the Swiss National Science Foundation (SNSF(CH)) through Grant No. 200021-117810, the NCCR MUST (to M.M.), the EU-COFUND program (to T.N.), and the University of Basel is also acknowledged.

[1]K. Yoshino, J. Esmond, and W. Parkinson, Chem. Phys. **221**, 169–174 (1997).
[2]W. Schneider, G. Moortgat, G. Tyndall, and J. Burrows, J. Photochem. Photobiol. A **40**, 195–217 (1987).
[3]T. Corcoran, E. Beiting, and M. Mitchell, J. Mol. Spectrosc. **154**, 119–128 (1992).
[4]U. Platt, D. Perner, G. Harris, A. Winer, and J. Pitts, Nature (London) **285**, 312–314 (1980).
[5]B. Finlayson-Pitts, L. Wingen, A. Sumner, D. Syomin, and K. Ramazan, Phys. Chem. Chem. Phys. **5**, 223–242 (2003).
[6]J. Calvert, G. Yarwood, and A. Dunker, Res. Chem. Intermed. **20**, 463–502 (1994).
[7]T. Schwartzentruber, L. Scalabrin, and I. Boyd, J. Spacecraft Rockets **45**, 1196–1206 (2008).
[8]S. Mishra and M. Meuwly, *Kinetics and Dynamics: From Nano- to Bio-Scale*, Challenges and Advances in Computational Chemistry and Physics Vol. 12 (Springer, Berlin, 2010).
[9]R. B. Gerber, V. Buch, and M. A. Ratner, J. Chem. Phys. **77**, 3022–3030 (1982).
[10]M. Beck, A. Jäckle, G. Worth, and H. D. Meyer, Phys. Rep. **324**, 1–105 (2000).
[11]H. Wang and M. Thoss, J. Chem. Phys. **119**, 1289–1299 (2003).
[12]T. Nagy, J. Yosa Reyes, and M. Meuwly, J. Chem. Theory Comput. **10**, 1366–1375 (2014).
[13]V. Kurkal, P. Fleurat-Lessard, and R. Schinke, J. Chem. Phys. **119**, 1489–1501 (2003).
[14]R. Jost, J. Nygrd, A. Pasinski, and A. Delon, J. Chem. Phys. **105**, 1287–1290 (1996).
[15]W. Bowman and F. De Lucia, J. Chem. Phys. **77**, 92–107 (1982).
[16]M. Ivanov, H. Zhu, and R. Schinke, J. Chem. Phys. **126**, 054304 (2007).
[17]L. Harding, H. Stark, J. Troe, and V. Ushakov, Phys. Chem. Chem. Phys. **1**, 63–72 (1999).
[18]H. Hippler, M. Siefke, H. Stark, and J. Troe, Phys. Chem. Chem. Phys. **1**, 57–61 (1999).
[19]V. Wakelam, I. Smith, E. Herbst, J. Troe, W. Geppert, H. Linnartz, K. Öberg, E. Roueff, M. Agndez, P. Pernot, H. Cuppen, J. Loison, and D. Talbi, Space Sci. Rev. **156**, 13–72 (2010).
[20]D. Angeli, Eur. J. Control **15**, 398–406 (2009).
[21]D. T. Gillespie, Annu. Rev. Phys. Chem. **58**, 35–55 (2007).
[22]D. T. Gillespie, J. Phys. Chem. **81**, 2340–2361 (1977).
[23]D. T. Gillespie, J. Comput. Phys. **22**, 403–434 (1976).
[24]W. Vance, A. Arkin, and J. Ross, Proc. Natl. Acad. Sci. U.S.A. **99**, 5816–5821 (2002).
[25]T. H. Dunning, J. Chem. Phys. **90**, 1007–1023 (1989).
[26]R. A. Kendall, T. H. Dunning, and R. J. Harrison, J. Chem. Phys. **96**, 6796–6806 (1992).
[27]H. Wener and P. Knowles, J. Chem. Phys. **82**, 5053–5063 (1985).
[28]S. R. Langhoff and E. Davidson, Int. J. Quantum Chem. **8**, 61–72 (1974).
[29]W. Duch and G. H. F. Diercksen, J. Chem. Phys. **101**, 3018–3030 (1994).
[30]H. J. Werner, P. J. Knowles, G. Knizia, F. R. Manby, and M. Schütz, WIREs Comput. Mol. Sci. **2**, 242–253 (2012).
[31]J. Vanderslice, E. Mason, and W. Maisch, J. Chem. Phys. **31**, 738–746 (1959).
[32]J. Vanderslice, E. Mason, W. Maisch, and E. Lippincott, J. Mol. Spectrosc. **3**, 17–29 (1959).
[33]D. D. Konowalow and J. O. Hirschfelder, Phys. Fluids **4**, 629–636 (1961).
[34]T. S. Ho and H. Rabitz, J. Chem. Phys. **104**, 2584–2597 (1996).
[35]M. Meuwly and J. Hutson, J. Chem. Phys. **110**, 3418–3427 (1999).
[36]D. S. Watkins, *Fundamentals of Matrix Computations*, 2nd ed. (Wiley, New York, 2002).
[37]W. Olver, D. Lozier, R. Boisvert, and C. Clark, *NIST Handbook of Mathematical Functions* (Cambridge University Press, New York, 2010).
[38]P. Soldan and J. M. Hutson, J. Chem. Phys. **112**, 4415–4416 (2000).
[39]T. Hollebeek, T.-S. Ho, and H. Rabitz, J. Chem. Phys. **106**, 7223–7227 (1997).
[40]K. K. Irikura, J. Phys. Chem. Ref. Data **36**, 389–397 (2007).
[41]L. Verlet, Phys. Rev. **159**, 98–103 (1967).
[42]R. L. Liboff, *Introductory Quantum Mechanics*, 4th ed. (Addison-Wesley, Massachusetts, 2003).
[43]R. N. Porter, L. M. Raff, and W. H. Miller, J. Chem. Phys. **63**, 2214–2218 (1975).
[44]R. D. Levine, *Molecular Reaction Dynamics* (Cambridge University Press, Cambridge, 2005).
[45]M. Brouard, *Reaction Dynamics*, Oxford Chemistry Primers Vol. 61 (Oxford Science Publications, Oxford, 1998).
[46]N. E. Henriksen and F. Y. Hansen, *Theories of Molecular Reaction Dynamics: The Microscopic Foundation of Chemical Kinetics*, Oxford Graduate Texts (Oxford University Press, Oxford, 2012).
[47]J. Duff and R. D. Sharma, J. Chem. Soc., Faraday Trans. **93**, 2645–2649 (1997).

[48]D. Frenkel and B. Smit, *Understanding Molecular Simulation: From Algorithms to Applications*, 2nd ed. (Academic Press, London, 2001).
[49]See supplementary material at http://dx.doi.org/10.1063/1.4897263 for the test of the *ab initio* calculations and of the prediction abilities of the RKHS procedure.
[50]A. Delon and R. Jost, J. Chem. Phys. **95**, 5686–5700 (1991).
[51]R. Georges, A. Delon, and R. Jost, J. Chem. Phys. **103**, 1732–1747 (1995).
[52]K. P. Huber and G. Herzberg, *Molecular Spectra and Molecular Structure. IV. Constants of Diatomic Molecules* (Van Nostrand, Princeton, 1979).
[53]J. Troe, Ber. Bunseng. Phys. Chem. **73**, 144–147 (1969).
[54]M. Rohrig, E. L. Petersen, D. F. Davidson, and R. K. Hanson, Int. J. Chem. Kinet. **29**, 483–493 (1997).
[55]H. Sabbah, L. Biennier, I. Sims, Y. Georgievskii, S. Klippenstein, and I. W. M. Smith, Science **317**, 102–105 (2007).
[56]I. R. Sims, Nat. Chem. **5**, 734–736 (2013).
[57]J. Zheng, X. Xu, R. Meana-Paneda, and D. G. Truhlar, Chem. Sci. **5**, 2091–2099 (2014).
[58]K. Glanzer and J. Troe, J. Chem. Phys. **63**, 4352–4357 (1975).